A novel visible-light-response plasmonic photocatalyst CNT/Ag/AgBr and its photocatalytic properties†

Yuanguo Xu,[a] Hui Xu,[a] Jia Yan,[b] Huaming Li,*[b] Liying Huang,[b] Qi Zhang,[b] Chuanjing Huang[c] and Huilin Wan[c]

A facile, one-step synthesis of carbon nanotube (CNT)-loaded Ag/AgBr is reported. The as-prepared samples were characterized by scanning electron microscopy (SEM), X-ray photoelectron spectroscopy (XPS), X-ray diffraction (XRD), UV/Vis absorption spectroscopy, Fourier transform infrared (FT-IR) spectroscopy, photoluminescence (PL) spectroscopy and electrochemical impedance spectroscopy (EIS). The CNT/Ag/AgBr composite exhibited much higher photocatalytic activity than pure Ag/AgBr in degrading methyl orange (MO) dye solution. The loading amount of CNT had a significant influence on the photoactivity of the CNT/Ag/AgBr composite. When the CNT loading amount was 1.4 at%, the hybrid material showed the highest photocatalytic ability. The result showed that a small amount of CNT was beneficial for photo-generated electron transfer, which could enhance the photoactivity of CNT/Ag/AgBr. The degradation dye solution was tested by liquid chromatography/mass spectrometry (LC/MS) and total organic carbon (TOC) analysis. Based on the results, the structure of the synthesized CNT/Ag/AgBr hybrid material was verified and the possible degradation path of the MO dye was proposed. A possible visible-light photocatalytic degradation mechanism was also discussed.

1 Introduction

Currently, environmental problems caused by organic pollutants have received a lot of attention. To deal with increasing pollution, photocatalytic technology using photocatalysts has been widely investigated, and various photocatalysts have been prepared.[1–3] Among these photocatalysts, plasmonic photocatalysts have been extensively investigated due to their excellent performance in photocatalytic degradation reactions, especially in the silver halide system,[4] which has been reported in many works (such as Ag@AgCl,[5–8] Ag@AgBr,[9–11] Ag@AgI[12]). The high photocatalytic activity of these catalysts is mainly ascribed to the surface plasmon resonance (SPR) effect of silver nanoparticles (Ag-NPs) and the interaction between Ag and AgX.

Thus, Ag/AgX is used as a dopant to modify TiO_2, Bi_2WO_6 and Al_2O_3, *etc.*,[13–21] to accelerate the separation of the electrons

and holes in the catalyst and hence the photocatalytic ability of hybrid materials can be enhanced. However, the low surface area of pure Ag/AgX is not good for its photoactivity. Plasmon-induced electron–hole pairs in Ag/AgX recombine before they arrive at the surface, leading to a loss of plasmonic photoactivity. It is therefore meaningful to fabricate a new hybrid material which can enhance the photocatalytic activity of the plasmonic photocatalyst.

In recent years, carbon nanotubes (CNTs) have become the focus of intense research because of their high chemical stability, strong mechanical strength, high activated surface area, and high conductivity. Up to now, numerous works have been devoted to the synthesis and applications of CNT hybrid materials. The hybrid materials are investigated and used in different areas. On one hand, there are a lot of studies on the synthesis of hybrid nanomaterials, where CNTs act as a support offering varied degrees of control over the particle size and distribution along the CNT.[22–25] Some works have concentrated on enhancing the thermal properties[26] or increasing the electrical conductivity of the composites.[27–29] On the other hand, CNTs are widely used in the catalytic area. The hybrid materials Ag/CNT[30] and TiO_2/CNT[31] were fabricated for killing bacteria. FeO_x/Pt/CNT,[32] TiO_2/CNT,[33–35] Pt/CNT,[36] Ag/CNT[37] *etc.* were prepared and used for oxidizing organic compounds. Recently, how to utilize the visible-light energy efficiently has

[a] *School of the Environment, Jiangsu University, 301 Xuefu Road, Zhenjiang, 212013, P R China*

[b] *School of Chemistry and Chemical Engineering, Jiangsu University, 301 Xuefu Road, Zhenjiang, 212013, P R China. E-mail: lihm@ujs.edu.cn; Fax: +86-511-88791108; Tel: +86-511-88791108*

[c] *State Key Laboratory of Physical Chemistry of Solid Surfaces, Xiamen University, Xiamen, 361005, P R China*

† Electronic supplementary information (ESI) available. See DOI: 10.1039/c3cp44104k

This journal is © the Owner Societies 2013

Phys. Chem. Chem. Phys., 2013, **15**, 5821–5830 | **5821**

attracted the public's attention. It is believed that carbon materials have some beneficial effects on the photocatalytic activity of TiO$_2$ by inducing synergies or cooperative effects between them. Lots of works have been reported on the preparation of CNT/TiO$_2$ hybrid materials[38–42] and their use for the photodegradation of azo dyes. There are also some other materials combined with CNTs being prepared and used as photocatalysts, such as CNT/ZnO,[43] CdS-CNT,[44] CNT/ZnS,[45] Ag/CNT[46] and some ternary compound materials like Pt/TiO$_2$/CNT,[47] Ag-CNT/TiO$_2$, etc.[48] All these works show that there is a synergetic effect between CNTs and the materials, and CNTs could change their intrinsic properties and thus enhance their performance.

However, no works have been reported on the modification of Ag/AgX with CNTs concerning the improvement of the photocatalytic ability of the plasmonic photocatalyst Ag/AgX. In this work, a novel CNT/Ag/AgBr composite structure with a small CNT loading amount was designed with the purpose of enhancing the photoactivity of Ag/AgBr. The possible mechanism of the effect of CNTs on the enhancement of visible-light performance was discussed. The degradation products of methyl orange (MO) solution were analyzed by LC/MS. Based on the LC/MS results, a possible degradation path was proposed.

CNT/Ag/AgBr was successfully synthesized by a simple one-step hydrothermal method. Ag/AgBr acted as the supporter and CNTs acted as the dopant material, which was different from other works. Compared with pure Ag/AgBr, the CNT/Ag/AgBr hybrid showed enhanced catalytic activity for the degradation of MO dye solution under visible-light irradiation, which was caused by the synergistic effect of SPR of Ag and the conductivity of CNTs which could lead to good electron transfer between the active materials. In addition, a possible photocatalytic mechanism was proposed based on the results.

2 Experimental

2.1 Materials and sample preparation

All chemicals were analytical grade and used as received without purification (graphite was chemically pure). CNTs (MWCNT–COOH, purity >95%) were purchased from Chengdu Organic Chemicals Co. Ltd., Chinese Academy of Sciences.

2.2 The synthesis of Ag/AgBr and CNT/Ag/AgBr

CNT/Ag/AgBr was prepared by a facile one-step hydrothermal method. In a typical synthesis procedure, three different solutions were prepared at first. Solution A: 100 mL of EG, 100 mL of water and 0.7150 g of CTAB were mixed and stirred. Solution B: 0.0050 g of CNT was put into 200 mL of solution A, and the mixture was stirred and ultrasonicated for 2 h to get a CNT dispersion solution. Solution C: AgNO$_3$ (0.1000 g) and urea (0.2885 g) were dissolved in a mixture which contained 30 mL of EG and 30 mL of water.

Ag/AgBr was prepared by mixing 60 mL of solution A and 60 mL of solution C, and then was transferred to 25 mL Teflon-lined stainless-steel autoclaves (each was filled with 20 mL) and kept for 4 h at 160 °C. After cooling to room temperature, the precipitate was washed and collected.

CNT/Ag/AgBr samples with different modified CNT contents were prepared by taking 4 mL, 12 mL, 32 mL of solution B, and adding 56 mL, 48 mL and 28 mL of solution A to the three kinds of solution respectively (CNT : AgNO$_3$ was 1 : 1000, 3 : 1000 and 8 : 1000 in mass ratio, and the molar ratios of CNTs in the composite were 1.4%, 4.1% and 10.2%, respectively). Then, the mixtures were transferred to 25 mL Teflon-lined stainless-steel autoclaves and kept for 4 h at 160 °C. After cooling to room temperature, the precipitate was washed and collected. The reference photocatalyst graphite/Ag/AgBr was prepared by the above-mentioned method (graphite : AgNO$_3$ was 1 : 1000 in mass ratio and 1.4% in molar ratio).

2.3 Characterization

The crystal phases of CNTs and CNT/Ag/AgBr powders were analyzed by XRD analysis using a Bruker D8 diffractometer with Cu-Kα radiation (λ = 1.5418 Å) in the 2θ range of 10°–80°. The SEM images of the samples were recorded using a JEOL JWSM-7001F field emission microscope. The UV-vis absorption spectra of the samples were measured under the diffuse reflection mode using a UV-vis spectrophotometer (UV-2450, Shimadzu Corporation, Japan). Fourier transform infrared (FT-IR) spectra of all the catalysts (KBr pellets) were recorded on a Nicolet Model Nexus 470 FT-IR instrument. X-ray photoemission spectra (XPS) were recorded on a PHI5300 with a monochromatic Mg Kα source to explore the elements on the surface. Photoluminescence (PL) spectra of the catalyst were measured using a QuantaMaster & TimeMaster Spectrofluorometer, QuantaMaster^{TM} 40 (Photon Technology International, Inc.). The samples were excited at a wavelength of 362 nm to measure the emission spectrum. The total organic carbon (TOC) content of the degradation dye was measured on a MultiN/C2100 TOC/TN (Germany). Electrochemical measurements were performed on an electrochemical workstation (CHI 660B Chenhua Instrument Company, Shanghai, China).

2.4 Photocatalytic activity test

The application of the CNT/Ag/AgBr composites to the degradation of organic dye MO was investigated under visible-light irradiation at room temperature. In a typical procedure, the reaction was carried out with 0.0200 g of photocatalyst suspended in 100 mL of MO solution. The concentration of the MO solution was 10 mg L^{-1}. Before the lamp (300 W Xe arc lamp equipped with an ultraviolet filter to provide visible light with $\lambda \geq 400$ nm) was turned on, the solution was stirred for 0.5 h in the dark to ensure the adsorption–desorption equilibrium between the photocatalysts and the dyes. The solution was sampled at 10 minute intervals and centrifuged, and the above liquid was then monitored by UV-vis spectroscopy at 463 nm. CNTs (0.0200 g) were put into MO solution first, and then they were collected and used after the absorption–desorption equilibrium was reached. The degradation of 4-chlorophenol was also tested and then monitored by UV-vis spectroscopy at 225 nm.

2.5 LC/MS analysis

Liquid Chromatography Mass Spectra (LC/MS) (LXQ Linear Ion Trap Mass Spectrometer) were used to analyze the degraded products.

The LC setup was equipped with two Varian ProStar210 pumps, an Agilent TC-C (18) column, and a Varian ProStar325 UV-Vis Detector at 254 nm. A solution of methanol and H_2O in the ratio 45 : 55 (v/v) was used as the mobile phase at 0.8 mL min^{-1}, and 20 μL of the sample solution was injected. The column oven temperature was 35 °C. The mass spectrometer was operated in negative polarity.

2.6 Electrochemical impedance spectroscopy (EIS)

EIS measurements were performed on an electrochemical workstation (CHI 660B Chenhua Instrument Company, Shanghai, China) based on a conventional three-electrode system comprised of indium-tin oxide glass (ITO) as the working electrode, platinum wire as the counter electrode, and Ag/AgCl (saturated KCl solution) as the reference electrode. The EIS measurements were performed in a 0.1 M KCl solution containing 5 mM $Fe(CN)_6^{3-}/(Fe(CN)_6^{4-}$ with a frequency range from 0.01 Hz to 10 kHz at 0.24 V, and the amplitude of the applied sine wave potential in each case was 5 mV. Modified ITO was used as the working electrode. The modified electrode was prepared by a simple method as follows: 5 mg Ag/AgBr was dispersed in 1 mL EG solution to make an Ag/AgBr homogeneous suspension. Then, 20 μL of the slurry was dripped on the ITO glass with a 1 cm × 0.5 cm area and dried at 60 °C for 8 h (denoted as Ag/AgBr/ITO). CNT/Ag/AgBr/ITO with the same quantities was prepared with the same procedure.

3 Results and discussion

Fig. 1 shows the XRD patterns of the CNTs and CNT/Ag/AgBr composites synthesized with different CNT contents. For the CNT/Ag/AgBr composite, the peak at 38.1° (marked with "♥") corresponding to the (111) crystal plane of Ag clearly represents the formation of Ag (JCPDS no. 04-0783). The peaks at 26.7°, 31.0°, 44.3°, 52.5°, 55.0°, 64.5° and 73.3° (marked with "●") are attributed to the (111), (200), (220), (311), (222), (400) and (420) crystal planes of AgBr (JCPDS no. 06-0438).[9,11,49] However, no obvious peaks for CNTs are observed in the composites by XRD, because the trace amount of loaded CNTs with a low atomic number cannot be resolved by XRD.[50] The existence of CNTs

can be determined by the following SEM-EDS analysis. Besides, the addition of CNTs does not change the diffraction peak positions of Ag and AgBr in the CNT/Ag/AgBr samples when compared with the JCPDS standard data of Ag and AgBr, which suggests that CNTs are not incorporated into the lattice of Ag/AgBr.

The morphologies of all products were characterized by SEM. Fig. 2a shows pure CNTs possess a nanoscale tubular morphology with diameters of ca. 20–30 nm, and various lengths. This may be because the nanotubes were broken in the ultrasonic dispersion process. Fig. 2b shows that pure Ag/AgBr is particulate in form, and the larger particles are AgBr and some of the small particles covering their surface are Ag NPs (as indicated by the arrows in Fig. 2b). In order to confirm that the small particles are Ag, electron backscatter diffraction (EBSD) was performed. Fig. S1(a) and (b) (ESI†) present an SEM image and a back scattering electron (BSE) image for the Ag/AgBr composite, in which both the (a) and (b) micrographs were taken in the same field. It is clear that in the BSE image (Fig. S1(b), ESI†), which is the same area as the SEM image (Fig. S1(a), ESI†), the small particles (in the circled area) distributed on the large particles are bright. Commonly, the backscattered electron signal increases with increasing atomic number (z) of the material. In other words, regions with heavier elements are brighter.[51,52] Therefore, the bright part shows the distribution of Ag particles because Br has a much smaller atomic number. The EBSD result indicates that the small particles on the surface of the large particles are Ag. The overall view of Ag/AgBr is shown in Fig. S1c (ESI†). It can be seen that the "large particles" are mainly in the range of 0.5–3 μm, and the "small particles" are mostly in the range of 50–100 nm.

The surface of the CNT/Ag/AgBr samples is rough after the addition of CNTs, which is different from that of pure Ag/AgBr (as indicated by the arrows in Fig. 2c–e). From the images of Fig. 2c–e, it can be clearly seen that more and more CNTs cover the surface of the hybrid with increasing CNT content. As can be seen in Fig. 2c, there are just a few CNTs on the surface of Ag/AgBr particles. When the content increases to 10.2 at%, a large number of CNTs can be seen in the junction area between particles and on the surface of the catalyst (see Fig. 2e) (in order to see CNTs more clearly, CNT/Ag/AgBr with a high CNT content of about 41.4 at% (CNT:AgNO₃ = 5 wt%) is shown in Fig. S2, ESI†).

In order to confirm the compositions of the catalysts, Ag/AgBr, CNT/Ag/AgBr 4.1 at% and CNT/Ag/AgBr 10.2 at% were measured by EDS, and the results are shown in Fig. 2f–h, respectively. From Fig. 2f, it can be seen that the Ag/AgBr catalyst consists of Ag, Br and Si. From Fig. 2g and h, it can be seen that the CNT/Ag/AgBr samples consist of C, Ag, Br and Si. The Si peak is mainly caused by the samples being dispersed on Si plate in EDS analysis. Therefore, it can be confirmed that Ag/AgBr only consists of Ag and Br, and the CNT/Ag/AgBr samples consist of C, Ag and Br. When the CNT doping amount is very low, the C peak is weak in the CNT/Ag/AgBr samples. However, there is no obvious C peak in pure Ag/AgBr, which confirms the existence of C element in the CNT/Ag/AgBr sample. With the EDS results and the size of the tubular material, it can be confirmed that the tubular material is CNT. The XRD and the EBSD results have
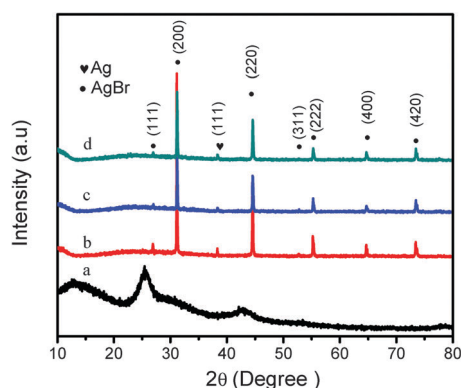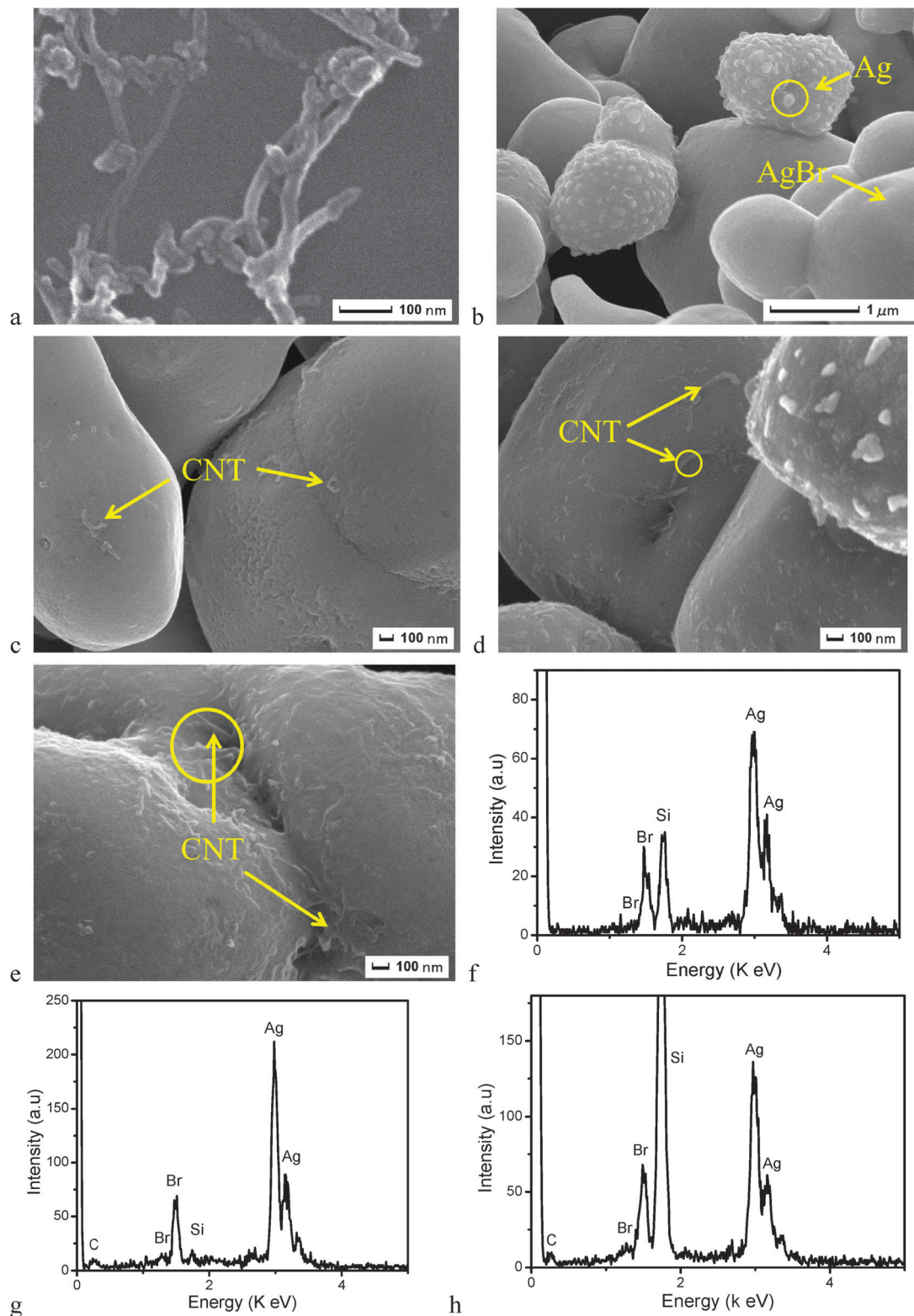

Fig. 1 XRD patterns of CNTs (a), 1.4 at% CNT/Ag/AgBr (b), 4.1 at% CNT/Ag/AgBr (c), 10.2 at% CNT/Ag/AgBr (d).

This journal is © the Owner Societies 2013

Phys. Chem. Chem. Phys., 2013, 15, 5821–5830 | 5823

Fig. 2 SEM images of CNTs (a), Ag/AgBr (b), 1.4 at% CNT/Ag/AgBr (c), 4.1 at% CNT/Ag/AgBr (d), 10.2 at% CNT/Ag/AgBr (e). Parts f, g and h are the EDS results of b, d and e respectively.

already confirmed the existence of Ag. So combining the results of SEM-EDS and XRD, it can be confirmed that CNT/Ag/AgBr has been successfully synthesized.

The elemental compositions of the catalysts were analyzed by XPS, and Fig. 3a displays the survey XPS spectrum of 1.4 at% CNT/Ag/AgBr, which mainly contains the peaks of Ag, Br, O and C.
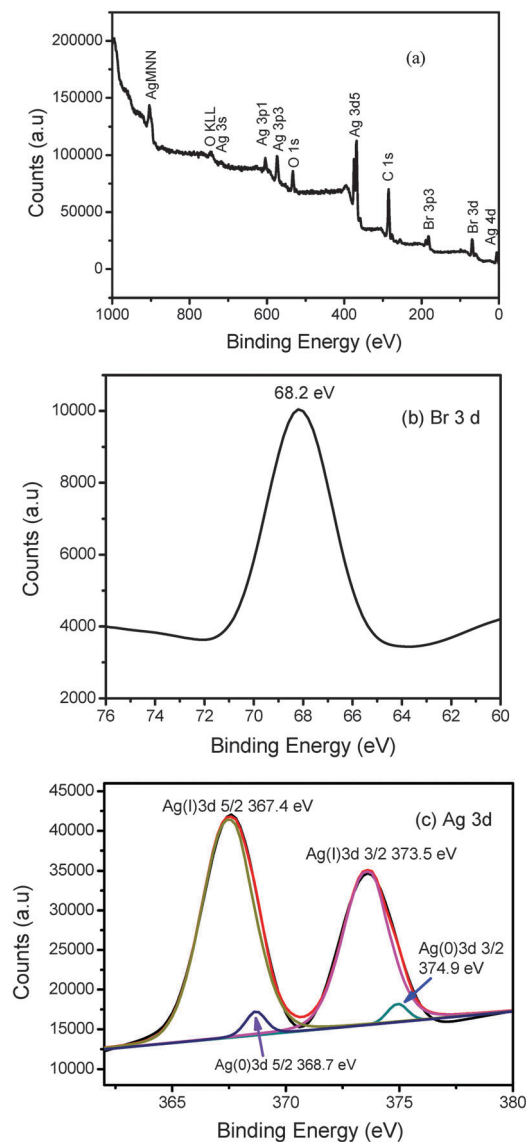
Fig. 3 XPS survey spectrum of CNT/Ag/AgBr (10.2 at%) composite (a), high-resolution XPS spectra of Br 3d (b) and Ag 3d (c).

Generally, a small amount of O may be due to surface adsorption of oxygen, and the C 1s peak is probably due to the CNTs and the adventitious hydrocarbon from the XPS instrument itself. The existence of CNTs has been confirmed in the SEM-EDS result. The high-resolution XPS spectrum of Br 3d (Fig. 3b) displays a band at about 68.2 eV. The high-resolution XPS spectrum of Ag 3d is shown in Fig. 3c. The two bands at about 373.6 eV and 367.6 eV can be attributed to Ag $3d_{3/2}$ and Ag $3d_{5/2}$. Ag $3d_{3/2}$ can be divided into two different peaks at 374.9 eV and 373.5 eV, and Ag $3d_{5/2}$ can be divided into two different peaks at 368.7 eV and 367.4 eV. The peaks at 374.9 eV and 368.7 eV are attributed to Ag^0, which confirms the existence of Ag^0. The peaks at 373.5 eV and 367.4 eV are attributed to the Ag^+ of AgBr.[17,49] Compared with pure metallic Ag (368.2 eV[53]) and Ag/CNT,[46,54] the peaks ascribed to Ag 3d in CNT/Ag/AgBr exhibit an obvious shift. They are also different to the binding
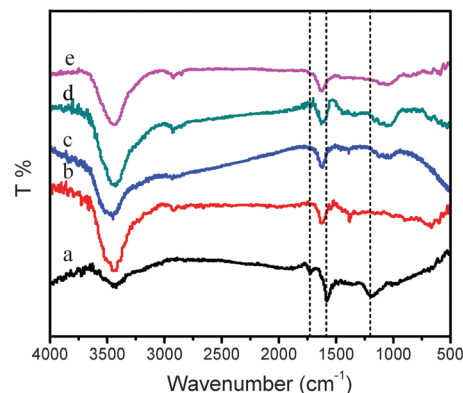
Fig. 4 FT-IR spectra of CNTs (a), Ag/AgBr (b), 1.4 at% CNT/Ag/AgBr (c), 4.1 at% CNT/Ag/AgBr (d), 10.2 at% CNT/Ag/AgBr (e).

energy of the Ag 3d peak for AgBr (368.0 eV).[55] The shift is probably due to the interactions between Ag, AgBr and CNTs. SEM-EDS results have confirmed the existence of CNTs, while the XRD, EBSD and XPS results have confirmed the existence of Ag^0 and AgBr and the interaction between them. As a result, it can be confirmed that the CNT/Ag/AgBr composite structure has been successfully synthesized.

FT-IR spectroscopy was used to characterize the CNTs, Ag/AgBr and different CNT/Ag/AgBr samples. All the FT-IR spectra of the samples are shown in Fig. 4. There is a strong, broad absorption band at about 3450–3500 cm^{-1}, which can be assigned to the bending vibrations of adsorbed molecular water and stretching vibrations of OH groups.[56] The peak at 1718 cm^{-1} is due to the C=O stretch.[57] The peak at 1579 cm^{-1} is due to the carboxylic COO^- stretching vibration.[22] The peak at about 1184 cm^{-1} is attributed to the C–C–O stretching vibration (see Fig. 4a). All these confirm that CNTs are –COOH functionalized CNTs. As indicated by the three vertical lines, the three typical peaks of –COOH are not observed in the CNT/Ag/AgBr composites (see Fig. 4b–e), which indicates that the –COOH was destroyed in the formation process[22] or the CNT amount was too small to be detected.

UV/Vis absorption spectra of the Ag/AgBr, 1.4 at% CNT/Ag/AgBr, 4.1 at% CNT/Ag/AgBr, 10.2 at% CNT/Ag/AgBr and CNTs samples are shown in Fig. 5. The main absorption of bare AgBr is in the range of 200–450 nm.[58–61] In this work, the Ag/AgBr and CNT/Ag/AgBr samples show strong absorbance in the visible region (at about 500–650 nm), which can be ascribed to the SPR effect of Ag NPs.[62–64] It further indicates the existence of Ag^0 in the composite catalyst. The CNT/Ag/AgBr samples show enhanced absorption in the visible region compared with pure Ag/AgBr, and the visible absorption intensity of the catalysts increases with the increase of the CNT content because CNTs are good light absorptive materials (as shown in Fig. 5e). A similar result has been reported by Yu.[65] However, the SPR absorption peak becomes unobvious when the CNT content reaches 10.2 at%. It is probably due to the fact that the superfluous CNT covers the surface of Ag/AgBr (see Fig. 2e) and absorbs the light, which hinders the light absorption of Ag/AgBr, which leads to the unobvious SPR absorption of 10.2 at%
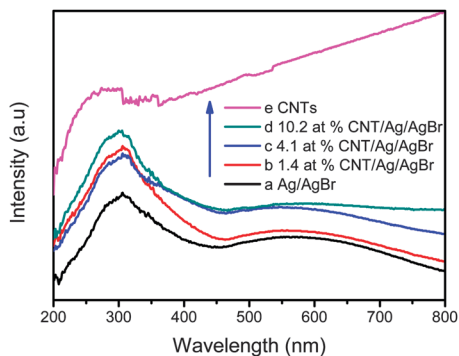
Fig. 5 UV/Vis absorption spectra of Ag/AgBr (a), 1.4 at% CNT/Ag/AgBr (b), 4.1 at% CNT/Ag/AgBr (c), 10.2 at% CNT/Ag/AgBr (d) and CNTs (e).

CNT/Ag/AgBr, and may be detrimental for the photocatalytic efficiency. Further observation indicates the absorption edge of CNT/Ag/AgBr exhibits a red-shift. The absorption edge shifting to the visible region means the increase in the visible-light harvesting capability of the CNT/Ag/AgBr catalysts.[66] This may be beneficial to increasing photocatalytic ability.

The photocatalytic activity of the as-prepared catalysts was evaluated by the degradation of MO under visible-light irradiation. Fig. 6a displays the degradation of MO in aqueous dispersions by different photocatalysts with the same weight of catalysts. The degradation efficiencies of MO are 0.6%, 75.4%, 87.7%, 79.1% and 61.1% for pure CNTs, Ag/AgBr, 1.4 at% CNT/Ag/AgBr, 4.1 at% CNT/Ag/AgBr and 10.2 at% CNT/Ag/AgBr after irradiation for 60 min, respectively. It can be seen that pure CNTs have no photocatalytic ability. The photoactivity of graphite/Ag/AgBr was also tested. 1.4 at% CNT/Ag/AgBr shows higher photoactivity than the conventional carbon material (1.4 at% graphite/Ag/AgBr) in the performance of degrading MO solution under visible-light irradiation (as shown in Fig. S3, ESI†). As can be seen from Fig. 6a, the CNT content has a significant influence on the photocatalytic degradation of MO dye, and the 1.4 at% CNT/Ag/AgBr sample shows the highest photocatalytic ability. The 1.4 at% CNT/Ag/AgBr sample improved by 20% compared with pure Ag/AgBr in 30 min, which indicates that MO can be degraded more efficiently by CNT/Ag/AgBr than by Ag/AgBr (see Fig. 6b and c). However, when the CNT content increases to 10.2 at%, the photocatalytic ability of the composite is lower than that of Ag/AgBr. The colorless pollutant 4-chlorophenol was also used as a target. The result of the degradation of 4-chlorophenol is shown in Fig. S4 (ESI†). It is obvious that the photolysis (without catalysts) of 4-chlorophenol can be neglected. It can be effectively degraded under visible light with the catalysts, and the degradation efficiencies are 52.9% and 54.6% for Ag/AgBr and 1.4 at% CNT/Ag/AgBr, respectively.

The linear relationship of $\ln(C_0/C)$ versus time is shown in Fig. 7. The corresponding kinetic constant (k) and regression coefficients (R^2) were calculated and are given in Table 1. The results indicate that the reaction followed first-order kinetics. The corresponding degradation rate constants (k) were estimated to be 0.02240 min^{-1}, 0.03552 min^{-1}, 0.02668 min^{-1}
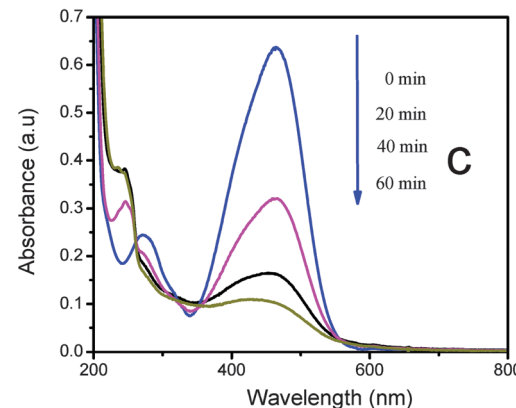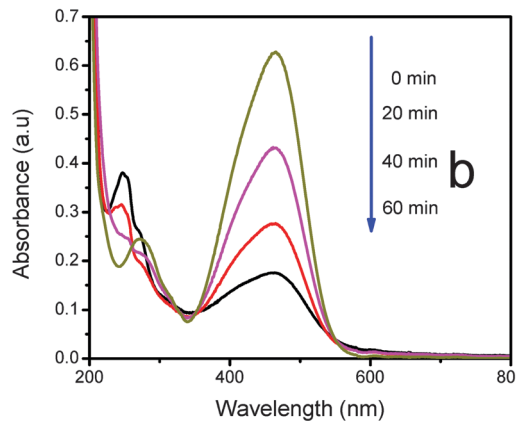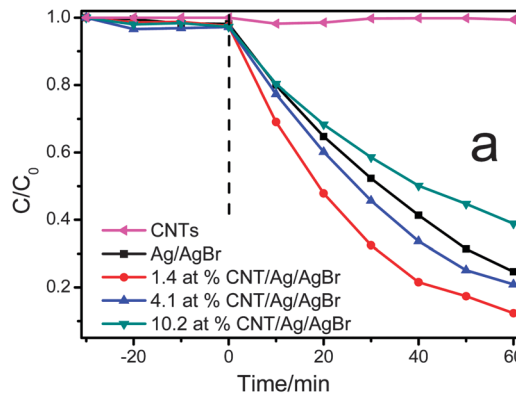

Fig. 6 Degradation of MO by different catalysts (a), and absorption spectral changes of MO by Ag/AgBr (b), and 1.4 at% CNT/Ag/AgBr (c).

and 0.01652 min^{-1}, respectively. The rate constant (k) of the CNT/Ag/AgBr (1.4 at%) photocatalyst was up to 1.59-fold faster than the bare Ag/AgBr.

It is interesting that a small CNT loading amount leads to enhanced photocatalytic ability, while a large CNT amount does not. As can be seen in Fig. 5 and 6a, the absorption intensity of the catalyst enhances with increasing CNT content because CNTs are good light-harvest materials.[67] But the photocatalytic ability of the catalyst decreases with the increasing absorption intensity when the CNT amount is larger than 1.4 at%. It is probably due to the fact that CNTs not only transfer electrons, but also absorb light at the same time, which prevents the
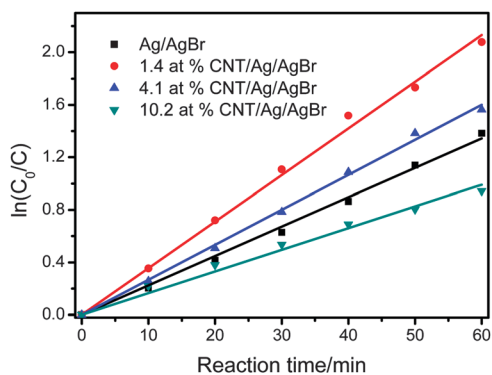
Fig. 7 The kinetics of MO degradation using various photocatalysts under visible-light irradiation.

Table 1 Kinetic constants and regression coefficients of MO degradation under visible-light irradiation

Sample	Kinetic constant (k, min^{-1})	R^2
Ag/AgBr	0.02240	0.99841
1.4 at% CNT/Ag/AgBr	0.03552	0.99837
4.1 at% CNT/Ag/AgBr	0.02668	0.99906
10.2 at% CNT/Ag/AgBr	0.01652	0.99507

visible light from being absorbed by Ag/AgBr.[68] In this work, the former factor is dominant for 1.4 at% CNT/Ag/AgBr and 4.1 at% CNT/Ag/AgBr, so the separated electrons from Ag/AgBr can be efficiently transferred, which leads to higher photoactivity. When the CNT content increases to 10.2 at%, CNTs become superfluous and the latter factor is dominant for 10.2 at% CNT/Ag/AgBr. The superfluous CNTs covering the surface hinders Ag/AgBr absorbing the light. In this case, although the addition of CNTs is good for the electron transfer, the total amount of separated electrons from Ag/AgBr will decrease. Thus, the photocatalytic ability of the catalyst decreases with increasing CNT content (despite the increase of absorption intensity in the visible region). This leads to the result that the photoactivity of 10.2 at% CNT/Ag/AgBr is lower than that of pure Ag/AgBr.

In order to investigate the degradation path, LC/MS was used to test the degradation products. The byproducts with different *m/z* values (304, 290, 157 and 173) were generated in the photocatalytic reaction by the two photocatalysts (Ag/AgBr and CNT/Ag/AgBr, Fig. S5, ESI†). This confirmed that the degradation path of the dye was the same in the presence of Ag/AgBr or CNT/Ag/AgBr.

Based on the above results, the possible structures of the byproducts with *m/z* 290, 157 and 173 and their possible degradation paths can be inferred. The degradation pathway is proposed in Fig. 8. The MO was demethylated in step (i) into 4-[4-(methylamino)phenylazo]benzenesulfonate (2), and then in step (ii) the intermediate could be degraded into benzenesulfonate (3) and 4-aminobenzenesulfonate (4).

TOC of the degraded solution after removing the catalyst for 1 h was also tested (Fig. S6, ESI†). The result shows that the decay of TOC is 1.3% and 7.2% for Ag/AgBr and CNT/Ag/AgBr respectively. The low mineralization may be caused by some byproducts being stable and difficult to decompose.

Many works about Ag/AgBr have been reported. Hu et al.[20] demonstrated that the electrons from plasmon-excited Ag NPs transferred to the conduction band (CB) of AgBr under visible-light irradiation through electrochemical methods. Huang et al.[69] reported that in the Ag/AgBr/BiOBr system, photogenerated electron–hole pairs were formed on the surface of Ag NPs owing to the SPRs. The electrons transferred from the photoexcited Ag NPs to the CB of AgBr. Zhang et al.[70] reported that in the AgBr@Ag system, the excitation energy overlapped with the localized SPR energy, which could excite Ag NPs to form surface plasmons. Thus, the SPR-induced oscillating electric fields were intensive enough to facilitate transfer of the plasmon energy to the nearby AgBr semiconductor for its excitation, which led to enhanced rates of radiative and/or nonradiative processes.

Based on the above analysis and the referenced published works, a logical reaction mechanism is proposed in Fig. 9. Both Ag NPs (SPR effect) and AgBr can be excited by visible-light.[20] Under visible-light irradiation, (I) photogenerated electron–hole pairs are formed on the surface of Ag NPs owing to the SPR effect. The electrons transfer from the photoexcited Ag NPs to the conduction band (CB) of AgBr,[20,69,70] and leave the positively charged Ag NPs^{n+}. (II) The electron–hole pairs in AgBr are separated and e$^-$ is excited from the valence band (VB) to the CB of AgBr, which creates holes (h$^+$) in the VB.[18] At the same time, parts of e$^-$ tend to shift to the positive potential Ag NPs^{n+}, and some Ag NPs^{n+} change into elemental Ag. (III) Many works about CNT and graphene hybrid materials have been reported,[71–75] and they possess the view that the electrons in the substrate transfer to CNTs, leading to electron–hole separation, which is beneficial for enhancing photoactivity. In this work, it is indicated that the addition of CNTs has a similar
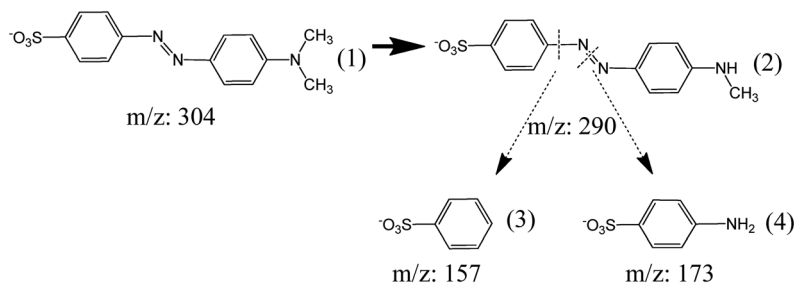
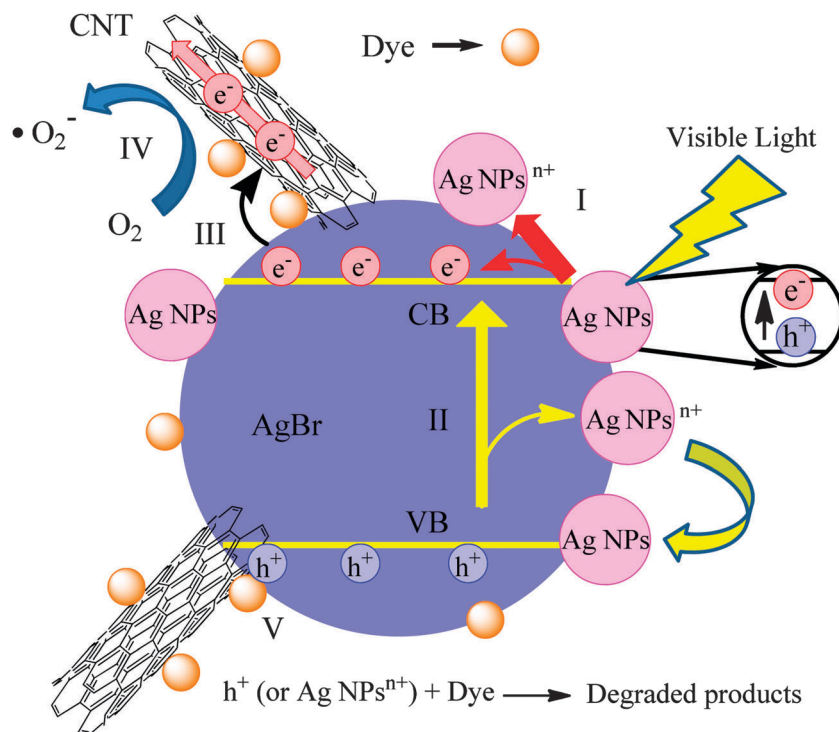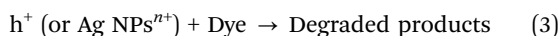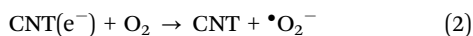**Fig. 8** The sequential degradation intermediate products and pathway.

Fig. 9 The proposed mechanism of the reaction process.

function to the reported works (it can facilitate the electron transfer and enhance the photoactivity of CNT/Ag/AgBr). So, it is suggested that e^- in the CB of AgBr ultimately transfers to the CNTs (III, eqn (1)) due to their good conductivity, and leads to the enhanced photoactivity. Then, the separated e^- and h^+ (and Ag NPs^{n+}) can react with the surface adsorbates O_2 (IV, eqn (2)) to generate highly reactive radical species[70] and oxidise the organic compounds into degraded products (V, eqn (3)), respectively.

$$CNT/Ag/AgBr + h\nu \rightarrow CNT(e^-)/Ag/AgBr(h^+) \quad (1)$$

$$CNT(e^-) + O_2 \rightarrow CNT + {}^\bullet O_2^- \quad (2)$$

$$h^+ (or\ Ag\ NPs^{n+}) + Dye \rightarrow Degraded\ products \quad (3)$$

In order to supply further evidence to support the proposed photocatalytic mechanism, PL of Ag/AgBr and 1.4 at% CNT/Ag/AgBr photocatalyst samples (as seen in Fig. 10) were tested, which revealed the photogenerated charge carrier separation and why the addition of CNTs could lead to enhanced visible-light activity for MO degradation. The emission peak intensity of the CNT/Ag/AgBr composite photocatalysts decreased, which suggested that the CNT/Ag/AgBr composite had a lower recombination rate of photo-generated charge carriers compared with Ag/AgBr. The efficient transfer of the electron could be ascribed to the doped CNTs, which were effective in electron–hole pair separation. This could be one reason why the CNT/Ag/AgBr photocatalyst exhibited higher activity for MO degradation than pure Ag/AgBr under visible light. EIS measurements were also employed to investigate the charge transfer resistance and the separation efficiency between the photogenerated electrons and
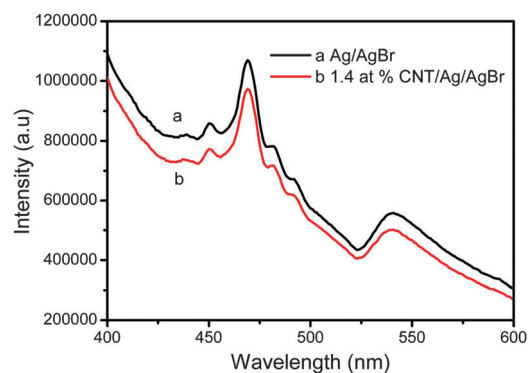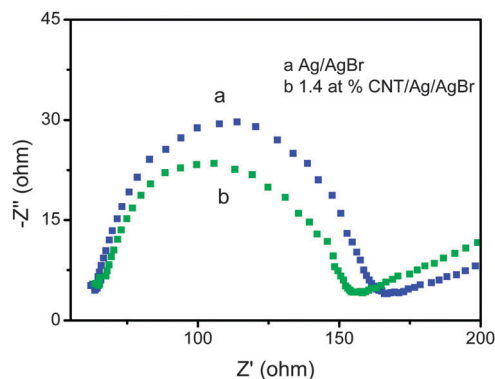

Fig. 10 PL spectra of Ag/AgBr (a), and 1.4 at% CNT/Ag/AgBr (b).

holes. From Fig. 11, it could be seen that the arc radius in EIS of CNT/Ag/AgBr is smaller than that of Ag/AgBr. This indicates that CNT/Ag/AgBr has a lower resistance than that of Ag/AgBr, which can accelerate the interfacial charge-transfer process.[76] Thus, the EIS result further supports that loading with CNTs facilitates the charge separation. In Chen's work,[63] they suggested that ${}^\bullet O_2^-$ was the main reactive species for the degradation of MO. This further indicated that the lower electron–hole recombination was beneficial to the enhanced photoactivity.

4 Conclusions

In summary, the novel visible-light-driven plasmonic photocatalyst CNT/Ag/AgBr composites with low CNT loading content (1.4–10.2 at%) were successfully synthesized by a one-step

Fig. 11 The electrochemical impedance spectra of Ag/AgBr/ITO (a) and 1.4 at% CNT/Ag/AgBr/ITO (b) in 0.1 M KCl solution containing 5 mM $Fe(CN)_6^{3-}$/($Fe(CN)_6^{4-}$.

hydrothermal method. The addition amount of CNTs had a significant influence on the photoactivity of Ag/AgBr. The as-prepared CNT/Ag/AgBr samples (with CNT loading <4.1 at%) showed better photocatalytic ability for the degradation of MO dye solution than pure Ag/AgBr. Among them, the 1.4 at% CNT/Ag/AgBr sample improved by 20% compared with pure Ag/AgBr in 30 min. The main reason for the enhancement of the photoactivity of CNT/Ag/AgBr was that the loading with CNTs promoted the separation of electron–hole pairs in the hybrid. However, the photocatalytic ability decreased with the increase of the CNT amount. Because the superfluous CNTs hindered Ag/AgBr's light absorption, there was a decreasing amount of separated electrons from Ag/AgBr, which ultimately resulted in the decreasing photocatalytic activity of the catalyst. Thus, the CNT/Ag/AgBr hybrid composite with low CNT content (<4.1 at%) was beneficial for the photocatalytic ability of the catalyst.

The degradation products of the dye solution were analyzed by LC/MS, and the degradation path could be confirmed. The synthesis of the CNT/Ag/AgBr composite with low CNT content could be extended to the fabrication of some other CNT–hybrid catalysts with low CNT contenst and their properties could be enhanced.

Acknowledgements

References

1 R. Asahi, T. Morikawa, T. Ohwaki, K. Aoki and Y. Taga, *Science*, 2001, **293**, 269.
2 J. W. Tang, Z. G. Zou and J. H. Ye, *Catal. Lett.*, 2004, **92**, 53.
3 K. Awazu, M. Fujimaki, C. Rockstuhl, J. Tominaga, H. Murakami, Y. Ohki, N. Yoshida and T. Watanabe, *J. Am. Chem. Soc.*, 2008, **130**, 1676.
4 P. Wang, B. B. Huang, Y. Dai and M. H. Whangbo, *Phys. Chem. Chem. Phys.*, 2012, **14**, 9813.
5 P. Wang, B. B. Huang, Z. Z. Lou, X. Y. Zhang, X. Y. Qin, Y. Dai, Z. K. Zheng and X. N. Wang, *Chem.–Eur. J.*, 2010, **16**, 538.
6 P. Wang, B. B. Huang, X. Y. Qin, X. Y. Zhang, Y. Dai, J. Y. Wei and M. H. Whangbo, *Angew. Chem., Int. Ed.*, 2008, **47**, 7931.
7 Y. P. Bi and J. H. Ye, *Chem. Commun.*, 2009, 6551.
8 Y. Y. Li and Y. Ding, *J. Phys. Chem. C*, 2010, **114**, 3175.
9 P. Wang, B. B. Huang, X. Y. Zhang, X. Y. Qin, H. Jin, Y. Dai, Z. Y. Wang, J. Y. Wei, J. Zhan, S. Y. Wang, J. P. Wang and M. H. Whangbo, *Chem.–Eur. J.*, 2009, **15**, 1821.
10 D. S. Wang, Y. D. Duan, Q. Z. Luo, X. Y. Li and L. L. Bao, *Desalination*, 2011, **270**, 174.
11 L. Kuai, B. Y. Geng, X. T. Chen, Y. Y. Zhao and Y. C. Luo, *Langmuir*, 2010, **26**, 18723.
12 C. H. B. Ng and W. Y. Fan, *J. Phys. Chem. C*, 2007, **111**, 2953.
13 M. Andersson, H. Birkedal, N. R. Franklin, T. Ostomel, S. Boettcher, A. E. C. Palmqvist and G. D. Stucky, *Chem. Mater.*, 2005, **17**, 1409.
14 J. G. Yu, G. P. Dai and B. B. Huang, *J. Phys. Chem. C*, 2009, **113**, 16394.
15 T. Morimoto, K. Suzuki, M. Torikoshi, T. Kawahara and H. Tada, *Chem. Commun.*, 2007, 4291.
16 C. Hu, Y. Q. Lan, J. H. Qu, X. X. Hu and A. M. Wang, *J. Phys. Chem. B*, 2006, **110**, 4066.
17 P. Wang, B. B. Huang, X. Y. Qin, X. Y. Zhang, Y. Dai and M. H. Whangbo, *Inorg. Chem.*, 2009, **48**, 10697.
18 L. S. Zhang, K. H. Wong, Z. G. Chen, J. C. Yu, J. C. Zhao, C. Hu, C. Y. Chan and P. K. Wong, *Appl. Catal., A*, 2009, **363**, 221.
19 L. S. Zhang, K. H. Wong, H. Y. Yip, C. Hu, J. C. Yu, C. Y. Chan and P. K. Wong, *Environ. Sci. Technol.*, 2010, **44**, 1392.
20 X. F. Zhou, C. Hu, X. X. Hu, T. W. Peng and J. H. Qu, *J. Phys. Chem. C*, 2010, **114**, 2746.
21 C. Hu, T. W. Peng, X. X. Hu, Y. L. Nie, X. F. Zhou, J. H. Qu and H. He, *J. Am. Chem. Soc.*, 2010, **132**, 857.
22 S. J. Guo, S. J. Dong and E. K. Wang, *Adv. Mater.*, 2010, **22**, 1269.
23 N. Chopra, W. W. Shi and A. Bansal, *Carbon*, 2011, **49**, 3645.
24 D. Eder and A. H. Windle, *J. Mater. Chem.*, 2008, **18**, 2036.
25 Z. Q. Tan, H. Xu, H. Abe, M. Naito and S. Ohara, *J. Nanosci. Nanotechnol.*, 2010, **10**, 3978.
26 I. Firkowska, A. Boden, A. M. Vogt and S. Reich, *J. Mater. Chem.*, 2011, **21**, 17541.
27 W. W. Zhang, W. L. Li, J. J. Wang, C. X. Qin and L. X. Dai, *Fibers Polym.*, 2010, **11**, 1132.
28 H. B. Du, Y. L. Li, F. Q. Zhou, D. Su and F. Hou, *J. Am. Ceram. Soc.*, 2010, **93**, 1290.
29 A. A. Eliseev, L. V. Yashina, M. M. Brzhezinskaya, M. V. Chernysheva, M. V. Kharlamova, N. I. Verbitsky, A. V. Lukashin, N. A. Kiselev, A. S. Kumskov, R. M. Zakalyuhin, J. L. Hutchison, B. Freitag and A. S. Vinogradov, *Carbon*, 2010, **48**, 2708.
30 J. H. Jung, G. B. Hwang, J. E. Lee and G. N. Bae, *Langmuir*, 2011, **27**, 10256.

31 O. Akhavan, M. Abdolahad, Y. Abdi and S. Mohajerzadeh, *Carbon*, 2009, **47**, 3280.
32 C. M. Zhou, Y. T. Chen, Z. Guo, X. Wang and Y. H. Yang, *Chem. Commun.*, 2011, **47**, 7473.
33 C. G. Silva and J. L. Faria, *Appl. Catal., B*, 2010, **101**, 81.
34 K. Zhang, F. J. Zhang, M. L. Chen and W. C. Oh, *Ultrason. Sonochem.*, 2011, **18**, 765.
35 N. Bouazza, M. Ouzzine, M. A. Lillo-Ródenas, D. Eder and A. Linares-Solano, *Appl. Catal., B*, 2009, **92**, 377.
36 J. M. Liu, H. Meng, J. I. Li, S. J. Liao and J. H. Bu, *Fuel Cells*, 2007, **7**, 402.
37 G. W. Yang, G. Y. Gao, C. Wang, C. L. Xu and H. L. Li, *Carbon*, 2008, **46**, 747.
38 M. J. Sampaio, C. G. Silva, R. R. N. Marques, A. M. T. Silva and J. L. Faria, *Catal. Today*, 2011, **161**, 91.
39 L. H. Tian, L. Q. Ye, K. J. Deng and L. Zan, *J. Solid State Chem.*, 2011, **184**, 1465.
40 P. N. Zhu, N. A. Sreekumaran, S. Y. Yang and R. Seeram, *Mater. Res. Bull.*, 2011, **46**, 588.
41 M. L. Chen, F. J. Zhang and W. C. Oh, *New Carbon Mater.*, 2009, **24**, 159.
42 W. Zhou, K. Pan, Y. Qu, F. F. Sun, C. G. Tian, Z. Y. Ren, G. H. Tian and H. G. Fu, *Chemosphere*, 2010, **81**, 555.
43 X. J. Wang, S. W. Yao and X. B. Li, *Chin. J. Chem.*, 2009, **27**, 1317.
44 A. H. Ye, W. Q. Fan, Q. H. Zhang, W. P. Deng and Y. Wang, *Catal. Sci. Technol.*, 2012, **2**, 969.
45 S. A. Feng, J. H. Zhao and Z. P. Zhu, *New Carbon Mater.*, 2008, **23**, 228.
46 Y. Yan, H. P. Sun, P. P. Yao, S. Z. Kang and J. Mu, *Appl. Surf. Sci.*, 2011, **257**, 3620.
47 W. C. Oh, F. J. Zhang and M. L. Chen, *J. Ind. Eng. Chem.*, 2010, **16**, 321.
48 F. J. Zhang, M. L. Chen and W. C. Oh, *New Carbon Mater.*, 2010, **25**, 348.
49 M. S. Zhu, P. L. Chen and M. H. Liu, *Langmuir*, 2012, **28**, 3385.
50 L. Ge and C. C. Han, *Appl. Catal., B*, 2012, **117–118**, 268.
51 F. J. Humphreys, *Scr. Mater.*, 2004, **51**, 771.
52 N. Hanada, E. Hirotoshi, T. Ichikawa, E. Akiba and H. Fujii, *J. Alloys Compd.*, 2008, **450**, 395.
53 D. D. Lin, H. Wu, R. Zhang and W. Pan, *Chem. Mater.*, 2009, **21**, 3479.
54 T. Liu, H. Q. Tang, X. M. Cai, J. Zhao, D. J. Li, R. Li and X. L. Sun, *Nucl. Instrum. Methods Phys. Res., Sect. B*, 2007, **264**, 282.
55 M. Yang, J. G. Zhao and J. J. Li, *Colloids Surf., A*, 2007, **295**, 81.
56 T. Tang, Z. X. Shi and J. Yin, *Mater. Chem. Phys.*, 2011, **129**, 356.
57 Y. L. Huang, C. C. M. Ma, S. M. Yuen, C. Y. Chuang, H. C. Kuan, C. L. Chiang and S. Y. Wu, *Mater. Chem. Phys.*, 2011, **129**, 1214.
58 J. Cao, B. D. Luo, H. L. Lin, B. Y. Xu and S. F. Chen, *J. Hazard. Mater.*, 2012, **217–218**, 107.
59 J. Cao, B. D. Luo, H. L. Lin and S. F. Chen, *J. Mol. Catal. A: Chem.*, 2011, **344**, 138.
60 S. Rodrigues, S. Uma, I. N. Martyanov and K. J. Klabunde, *J. Catal.*, 2005, **233**, 405.
61 L. Kong, Z. Jiang, H. H. Lai, R. J. Nicholls, T. C. Xiao, M. O. Jones and P. P. Edwards, *J. Catal.*, 2012, **293**, 116.
62 H. Xu, H. M. Li, J. X. Xia, S. Yin, Z. J. Luo, L. Liu and L. Xu, *ACS Appl. Mater. Interfaces*, 2011, **3**, 22.
63 H. L. Lin, J. Cao, B. D. Luo, B. Y. Xu and S. F. Chen, *Catal. Commun.*, 2012, **21**, 91.
64 P. Wang, B. B. Huang, X. Y. Zhang, X. Y. Qin, Y. Dai, Z. Y. Wang and Z. Z. Lou, *ChemCatChem*, 2011, **3**, 360.
65 J. G. Yu, J. J. Fan and B. Cheng, *J. Power Sources*, 2011, **196**, 7891.
66 C. H. Sun, A. Mukherji, G. Liu, L. Z. Wang and S. C. Smith, *Chem. Phys. Lett.*, 2011, **501**, 427.
67 S. Wang, Z. Y. Zhang and L. M. Peng, *Chin. Sci. Bull.*, 2012, **57**, 149.
68 J. G. Yu, T. T. Ma and S. W. Liu, *Phys. Chem. Chem. Phys.*, 2011, **13**, 3491.
69 H. F. Cheng, B. B. Huang, P. Wang, Z. Y. Wang, Z. Z. Lou, J. P. Wang, X. Y. Qin, X. Y. Zhang and Y. Dai, *Chem. Commun.*, 2011, **47**, 7054.
70 J. Jiang, H. Li and L. Z. Zhang, *Chem.–Eur. J.*, 2012, **18**, 6360.
71 Q. J. Xiang, J. G. Yu and M. Jaroniec, *J. Phys. Chem. C*, 2011, **115**, 7355.
72 Y. K. Kim and H. Park, *Appl. Catal., B*, 2012, **125**, 530.
73 J. Zhang, J. G. Yu, M. Jaroniec and J. R. Gong, *Nano Lett.*, 2012, **12**, 4584.
74 W. D. Zhang, L. C. Jiang and J. S. Ye, *J. Phys. Chem. C*, 2009, **113**, 16247.
75 J. C. Liu, H. W. Bai, Y. J. Wang, Z. Y. Liu, X. W. Zhang and D. D. Sun, *Adv. Funct. Mater.*, 2010, **20**, 4175.
76 S. B. Zhu, T. G. Xu, H. B. Fu, J. C. Zhao and Y. F. Zhu, *Environ. Sci. Technol.*, 2007, **41**, 6234.